ISSN No:-2456-2165

Development and Characterization of NiTiCu Alloy using Powder Metallurgy Route

Waheed Gul[1], Taseen Haider Roshaan[2], Zain Rashid[3]
[1*,2,3]Department of Mechanical Engineering,
Institute of Space Technology, Islamabad 44000, Pakistan

Ali Faiz[4], Aqib Ali[5]
[4,5]Department of Aerospace Engineering,
Institute of Space Technology, Islamabad 44000, Pakistan

Abstract:- In this research, TiNiCu alloys are developed using the powder metallurgy route. Two batches are prepared with varied compositions. Sample one holds Ti50 Ni50 by atomic weight. Ti50 Ni45 Cu5 composition is set for second sample and Ti50 Ni40 Cu10 for the preparation of third sample. The treatment of both the batches are done in different environmental conditions. Treatment in atmosphere and vacuum give different porosity values to the alloy samples. For sample with 0% Cu percentage the porosity achieved is 30.3%. The porosity achieved in case of 5% and 10% Cu atomic percentage is 27.3% and 31.56% respectively. The development methodology is opted based on the ability to produce porous alloys of varied grain sizes and densities. Several other techniques like Vacuum Arc Melting, Spark plasma Sintering are also used in the industry for obtaining high porosity levels in the developed SMA alloys. Here, the effect of variation of porosity on other mechanical and physical markers is also studied. Non-destructive characterization techniques are implied to identify the developed NiTi alloys and to access the behavior. XRD, DSC and Micro-hardness tests are performed and the results are analysed and compared with the previous research studies. The hardness values for batch one in case of sample one was 111Hv scale and it increases to 374Hv when the copper percentage increases to 5%.

Keywords:- *Shape memory alloys, Powder metallurgy, Porosity reduction, Non Destructive testing.*

I. INTRODUCTION

The surmounting growth in the field of science and technology resulted in the applicability of special materials in varied fields of application in industries, medicine and aerospace. Shape memory Alloys have found their true calling in the field of Medical for making orthodontics files, archwires and implants. The porous alloys allow for greater Compressive strength, high resistance to surface wear and great Biocompatibility and Cyto-compatibility.

The work of variation in the composition of alloying powder helps in changing the transition temperatures, porosity and ductility at a certain temperature. The changing of atomic composition can do work for the variation so much that certain treatment methods are to altered, modified and catered to obtain the right alloy having optimum shape memory effect.

The preparation of the samples has been done using the powder metallurgy route. Shape memory alloys are considered smart materials because of their ability to recover their shape when heated and cooled subsequently and hence making their applications spread across different cases, situations, and circumstances.

These materials show different behavior chemically and mechanically when processed differently under many different conditions. These alloys show pseudo-elasticity and shape memory effect. Pseudo-elastic behavior allows for the elastic nature of stress response. Whereas the shape memory effect is the property due to which it remembers its previous shape before heating and then comes back to its original form when cooled and vice versa.

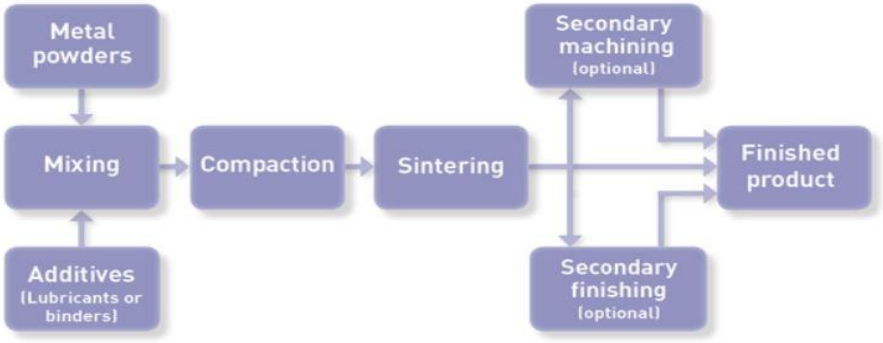

Fig. 1: Manufacturing processes involved in Powder Metallurgy

A series of steps are defined based on our sole aim of reducing the porosity of our alloy samples. The porosity is a function of the Sintering cycle, compaction pressure as well as Sintering conditions. The steps are defined based on the research study.

A result-oriented composition of alloys is defined as a depiction of variation of physical and mechanical properties. The samples are divided into two categories one serves as a control group for the other. The categorization is as such that the sets of two are defined based on the atomic weights of the species in the alloys. These alloys are in composition in order of:

- Sample 1 Ti50 Ni50
- Sample 2 Ti50 Ni45 Cu5
- Sample 3 Ti50 Ni40 Cu10

The decision of selection of the composition of the Shape memory alloy samples is based on the hardness increase with copper increase and porosity reduction when it is in a controlled environment. In addition, the corrosion is reduced to a minimum after the percentage of copper exceeds 8% in the SMA alloy samples.

II. MATERIALS AND METHODS

A. Materials

Powders of Ni, Ti and Cu are utilized having purity up to 99.00%. The powders were analyzed using Scanning Electron microscope (SEM). These materials were procured from the chemistry department of Peshawar UET, Pakistan.

B. Design parameters

The mixing is done based on the atomic weights and compositions are selected using the copper addition through a research paper to get a myriad of different results.

The samples were compressed under 500 MPa which is considered an intermediate pressure value to look for the porosity obtained in the green bodies.

The sintering conditions are selected on the impact of sintering on the porosity levels of the specimen and two different batches were sintered at different environmental conditions.

By sintering an alloy at 980□ Celsius and holding a temperature of 2 hours the porosity reached in the case is 53.6% [21]. Thus, the sintering temperature set for the reduction of the porosity is set to be 950 degrees Celsius to keep the porosity minimum.

The ratio of pore volume to the total volume is called green porosity which can be determined from the following equation:

$$P_g = (1 - P_g/P_{th}) * 100$$

Where Pg – green porosity percentage (g/cm3)

Pth is the theoretical density of bulk material (g/cm3). It can be calculated by the weight percentages of elemental powder multiplied by its theoretical density as follows:

$$\rho_{tB} = \sum_{i=1}^{n} Wt_1 * \rho_1 + Wt_2 * \rho_2 + Wt_3 * \rho_3 + \ldots\ldots\ldots + Wt_n * \rho_n$$

P1, 2…, n: theoretical density of elemental powder (g/cm3)

Wt1, 2… n: Weight percentage (%) of elemental powder in the alloy.

C. Preparation of TiNiCu Alloys

➢ *Mixing and Composition of TiNiCu Alloys*

The atomic weightage is calculated using tables of weight to atomic mass conversion The weighing of the samples is done in a weight balance using a container of weight 11.1 grams. Can + Powder = 129grams. Similarly, the zero error is interpolated for other powdered samples, then the compositions are collected and weighed based on 44.92% weight = Ti50 and Ni50 weight= 55.08%.

A sample of weight 5g is prepared for the development of billets of TiNiCu alloys. This is achieved based on making a mixture of 10 grams of each sample.

- For the first sample, 4.49 grams of Ti and 5.508 grams of Ni are used, No amount of copper is added to it.
- For Ti50 Ni45 Cu5, the weights taken were Ti=4.47grams Ni=4.93 grams and Cu=0.5grams.
- Ti50 Ni40 Cu10 the weights taken were Ti=4.45 grams Ni =4.36 grams and Cu= 1.18 grams.

Different spatulas are kept for the buckets to keep track of the composition. The buckets are kept closed with samples after weighing. The theoretical density of the samples is to be defined based on the density of the species present inside the sample multiplying with the weight percentage of the species (Ti, Ni, and Cu).

➢ Milling of TiNiCu Alloys

The next step is to identify the milling procedure which involves the mixing of the samples using rollers at a certain speed for proper mixing of the samples for a certain time. The variation in the time does impact the homogeneity of the mixture.

The speed and the time period of rotation are set for the mixtures. A ball mill machine is used in the mixing of samples. Balls are for grinding and rotation is for the mixing of the different powders together.

ISSN No:-2456-2165

Fig. 2: Mixing of Powder Samples

The bucket was selected to be play-free and non-compressible so that the mixing is not impacted by the compression because it is intact with the rollers which can compress the bucket hence glass containers were used in the procedure. The running speed V is set to be 40 rpm. The time was set to be 4 hours for proper mixing.

➢ *Compaction of Alloys*

Table 1: Billet Dimensions

Sample No	Compaction Pressure (MPa)	Height of billet (mm)
1	500	11.03
2	500	11.13
3	500	11.34

After the mixing of samples, the samples are set to be 5 grams for compaction in accordance with the 11mm die available for the hydraulic compaction machine. The compressor is managed to impart pressure upside down uniformly. Also, the press can be hydraulically and mechanically operated. In our case, we used a hydraulic machine with a cylindrical die of 11mm.

Single side compaction is done thus the surface finish on both the face surfaces are different and also thus homogeneity is reduced in this case as opposed to if we have implied upper and lower punches for our metal alloy powder The pressure value is set to be 500 MPa and then the compaction is initiated using the lab facilities in KRL, Islamabad. The green samples were prepared for both batches A, B.

The green samples are obtained and their dimensions are calculated. These green samples have some level of porosity in them which is then reduced when exposed to sintering.

➢ *Sintering Cycle of two batches of Alloys*

The Apparatus used in our sintering procedure is **Kejia Tube Furnace model KJ-1600vF** which is used in conjunction with other components.

- Vacuum two-stage compressor
- Argon cylinder
- Crucible (Ceramic, Alumina)

Two sintering cycles are implied to achieve the goal of reducing the porosity levels of the shape memory alloys developed through powder metallurgy.

Fig. 3: Sintering of Alloys

The conditions for the first cycle are as follows:

- The cycle is oriented to sinter the samples at atmospheric conditions.
- The input is interpolated on the dial for the time of the cycle.
- Heating rate is then set which is kept at 5□ Celsius.
- Both the ends are tightened for negating any thermal losses after sample stacking on the crucible.

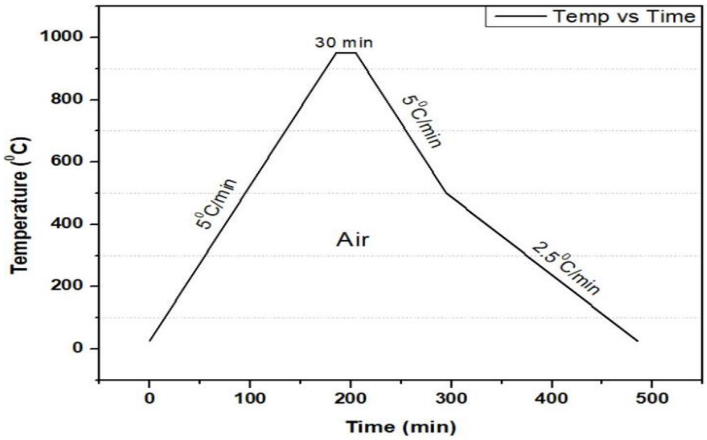

Fig. 4: Sintering cycle for Batch A samples

The conditions for the second cycle are as follows:

- The cycle is oriented to sinter the samples in inert and vacuum conditions.
- The input is interpolated on the dial for the time of the cycle
- Heating rate is then set which is kept at 5□ Celsius
- The vacuum compressor is set up till 120□ Celsius and then it is splashed with argon the vacuum pressure drops to -0.051 from -0.093 MPa of Vacuum pressure
- The rest of the cycle is made to run through the sintering tube with a flow of argon as an inert gas to prevent the reaction of species with oxygen and get contaminated.
- The samples are stacked on the alumina and SiO_2 crucible and both the ends are tightened for negating any thermal losses.

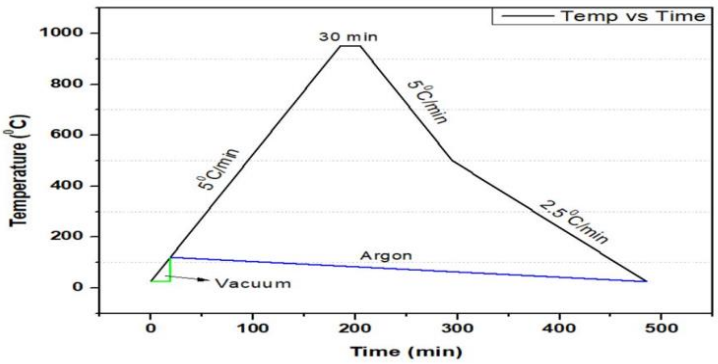

Fig. 5: Sintering cycle for Batch B samples

➢ *Prepared Alloys after Sintering*

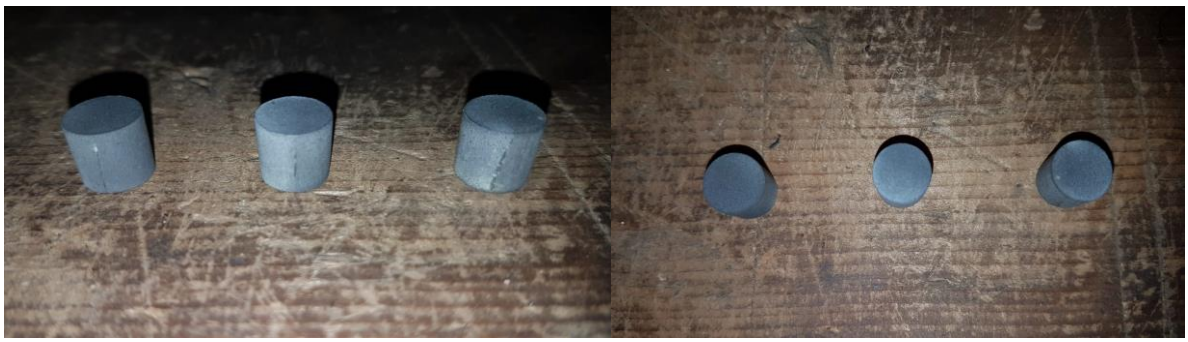

Fig. 6: Prepared Alloys

D. Porosity Reduction

The minimum amount of porosity up to 27% is observed due to the controlled environment of Vacuum and Argon in the 2nd sample of batch B which contains 5% of Cu. The exact amount of porosity levels are shown in the table and the graph below.

Table 2: Effect of Cu on Porosity

Cu (%)	Porosity (%)
0	30.3
5	27.3
10	31.56

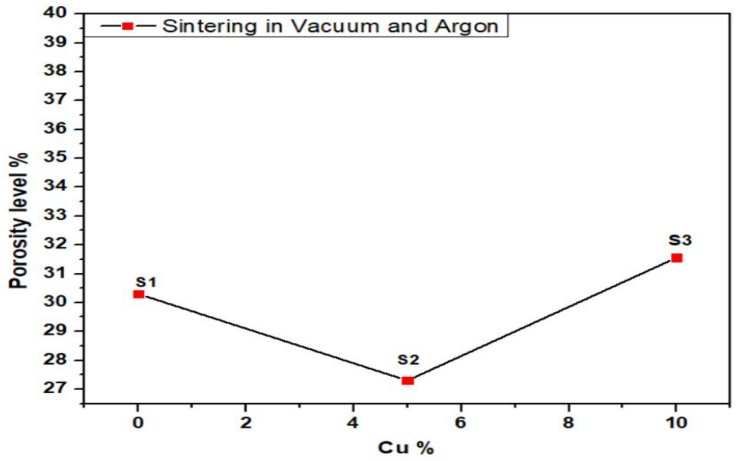

Fig. 7: Porosity Reduction

E. Characterization of Alloys

Different Characterization techniques are applied in order to develop an understanding of the behavior of the SMA alloys developed.

➢ *XRD Technique*

The machine which was utilized uses Cu-K source and (= 1.54A). The JCPDs card number helps identify the phases present in the sample, which contains both the primary and the secondary phases.

➢ *DSC Technique*

The heating of samples between ranges of -50 and 150 causes the phase to turn austenitic in nature in our case where these samples are characterized on DSC, **Mettler Toledo Switzerland Model DSC 823e.**

➢ *Micro Hardness Test*

A microhardness test has been performed on samples 1 and 2 of batch A to get the hardness value HV. The indentation is made along the surface distant from each other and the results are collected.

III. RESULTS AND DISCUSSION

A. XRD Pattern of Batch A Alloys

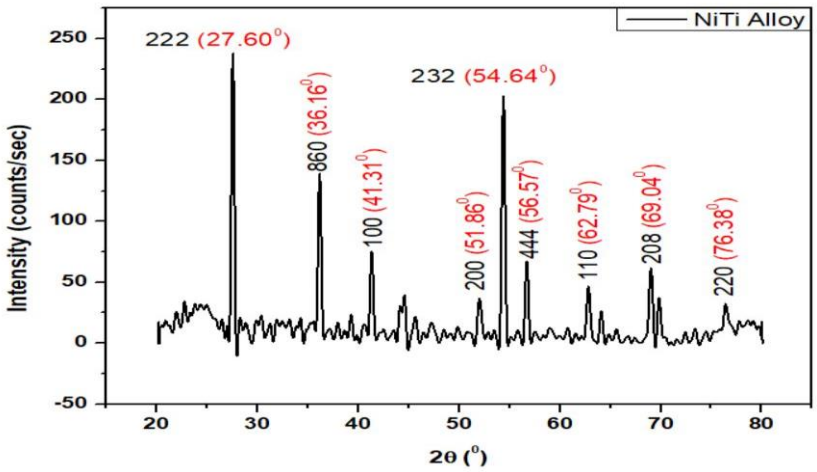

Fig. 8: XRD Pattern of Sample 1 (NiTi Alloy)

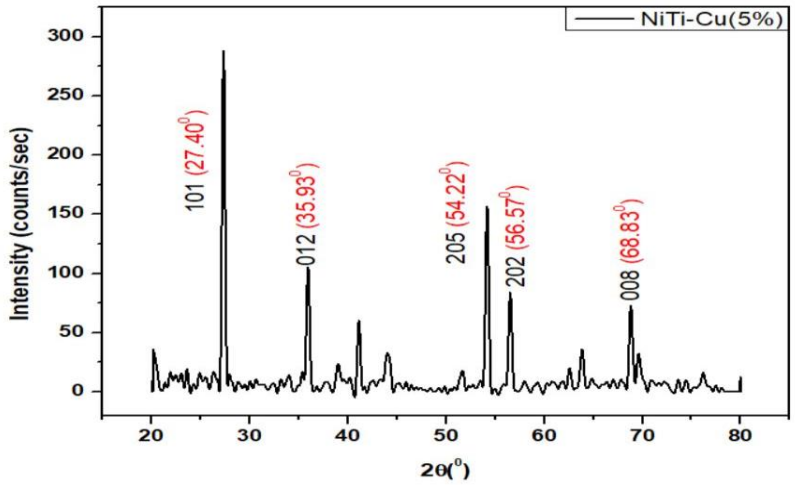

Fig. 9: XRD Pattern of Sample 2 (NiTiCu5%)

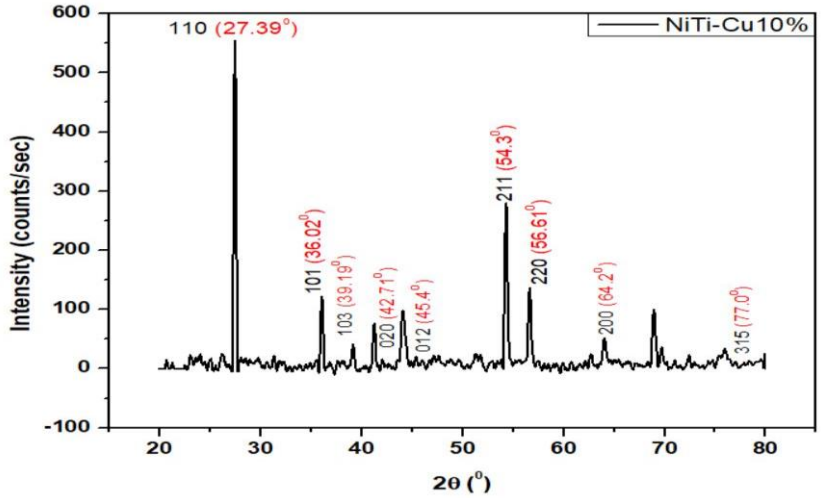

Fig. 10: XRD Pattern of Sample 3 (NiTiCu10%)

The variation in the porosity of the samples is validated through the graph. As the titanium is vaporized in sintering, it induces a Ni-rich sample and the species produced in the final form contains secondary phases, which is the result of porosity.

During the Batch B sintering in the presence of inert gas, argon plays its part, and thus not evaporating the titanium renders the sample to be less porous as if to compare it with the atmosphere. Otherwise, sintering in a vacuum causes the titanium to evaporate at much lower temperatures than 1668□-Celsius at 760mmHg.

B. SEM Results of Sample Powders

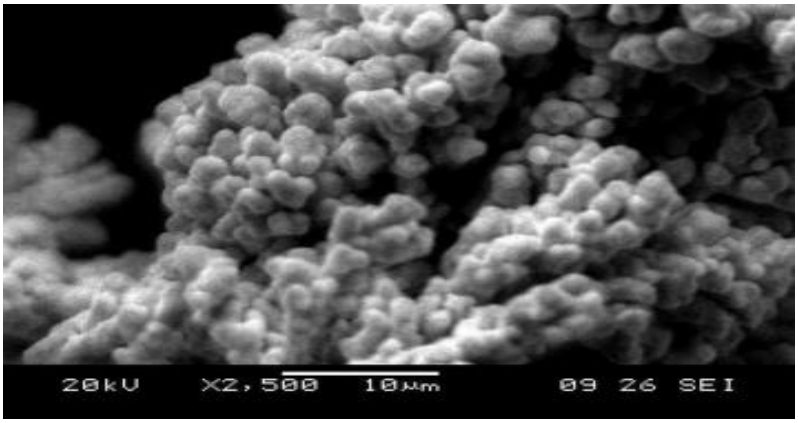

Fig. 11. SEM results of Cu Powder

The SEM image of copper powder presents the morphology of rounded bodies. The shape variation is not that steep as compared to Ti crystals. The magnification x2500 is set for the sample.

Table 3. The pore size of Cu powd**er**

Sr. no	Area (µm)	Mean (µm)	Min (µm)	Max (µm)	Angle (degree)	Length (µm)
1	0.227	148.144	94.944	197.95	86.309	1.489
2	0.372	164.416	141.75	193.193	-91.146	2.396
3	0.351	175.61	154	198	150.255	2.318
4	0.207	127.471	120.667	132.34	180	1.342
5	0.248	152.571	127.583	175.233	17.879	1.561
6	0.289	135.286	116.923	161	4.399	1.874
7	0.393	157.225	114	207.5	137.291	2.543

Pore sizes are obtained using the images from SEM and then processing it with software to look for the size and length of the pores at varied different angles. The size of the pores is measured by marking and comparing them with 10 micrometer scale. The scale gives us values at varied locations and tells us about the symmetry of the particles which are round in shape.

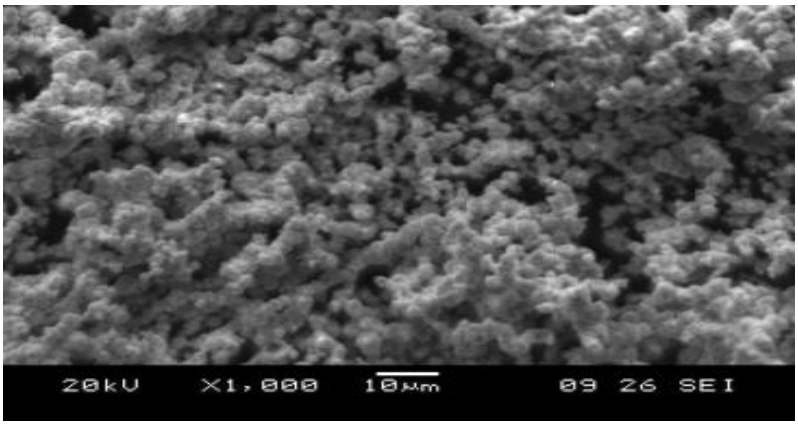

Fig. 12: SEM results of Ni Powder

The Nickel powdered is looked at using MIRA3 TESCAN for the powder texture is rounded pores and smaller is size using a scale of 10 micro meter.

Table 4: Pore size of Ni Powder

Sr. no	Area (µm)	Mean (µm)	Min (µm)	Max (µm)	Angle (degree)	Length (µm)
1	1.234	126.088	100.286	149.71	49.399	2.793
2	1.234	151.09	134.113	166.199	-164.476	2.829
3	0.96	120.237	111.22	129.184	30.256	2.104
4	1.097	116.971	112.672	121.14	0	2.423
5	0.96	166.949	153.476	178.865	23.199	2.307
6	1.234	113.124	34.318	177.363	-90	2.877
7	1.097	126.051	98	138.417	2.603	2.718

The nickel powder is also processed using ImageJ software and the sizes were grated using 10 micrometer scale. The variation in size is not very steep. The average length size is above 2.5 micrometers.

ISSN No:-2456-2165

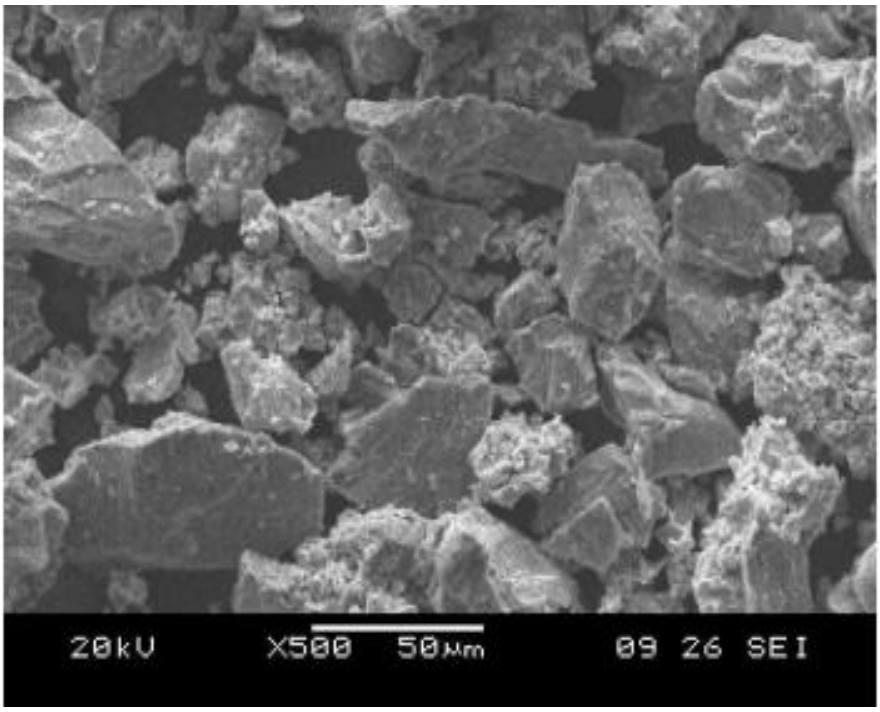

Fig. 13: SEM results of Ti Powder

The SEM results show the morphology of the powdered sample of Titanium which shows variation in the size of the crystals. Shape edges of crystals are visible along with more rounded shapes.

Table 5: The pore size of Ti Powder

Sr. no	Area (µm)	Mean (µm)	Min (µm)	Max (µm)	Angle (degree)	Length (µm)
1	37.496	108.705	86.937	181.457	42.93	50.627
2	16.07	104.63	92.645	144.684	32.412	21.444
3	15.534	117.155	91.003	162.26	63.435	20.561
4	12.856	88.988	80.86	102.114	90	16.666
5	14.998	111.826	91.773	181.088	90	20.115
6	14.463	137.864	87.397	212.378	105.101	18.751
7	17.141	115.123	59.32	163.147	127.164	22.356

The usage of ImageJ software allows us to better look at the sizes of the crystals of the powder utilized in the development of Alloys, The variation in size is greater than that of the other powdered samples.

C. SEM Results of Batch A Alloys

These results are based on the testing done using the FESEM TESCAN, housed in the material department of IST, Islamabad. The results are obtained at different powers, hence gives us leverage to better observe the species present in billet samples of batch A alloys. The images are compared with the literature observations and conclusions are drawn.

ISSN No:-2456-2165

Batch A (Sample 1)

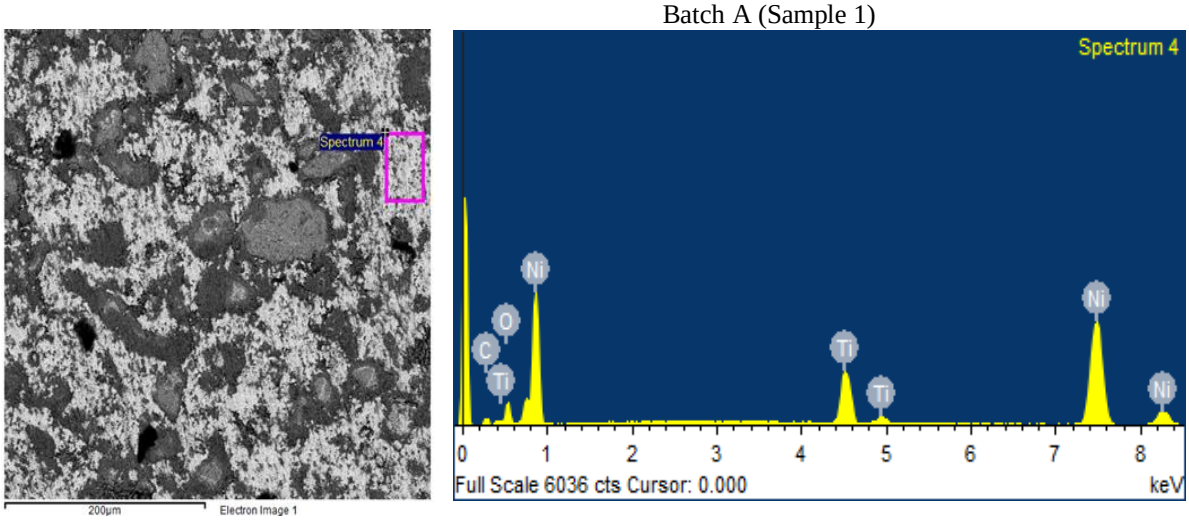

Fig. 14: SEM results of sample 1

This sample when looked at the whitish shade of it represents the positioning of species which accounts for a greater concentration of Ni present in the alloy. The images are taken and species presence shows that the alloy has varying concentrations of different metallic species spread across the surface. The results also show the presence of Ni, Ti, and O as external agents which seeps into results.

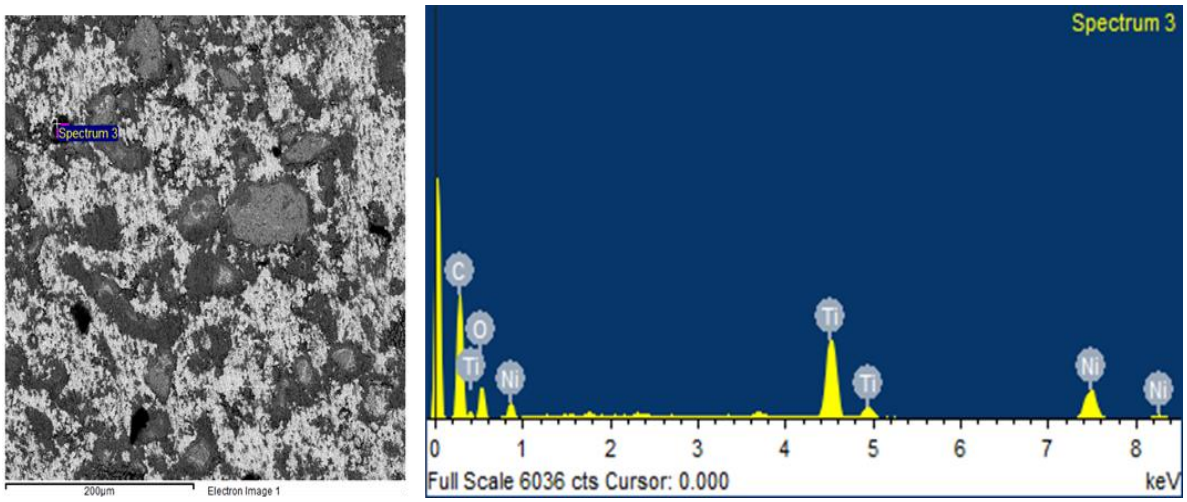

Fig. 15: SEM results of sample 1

This image shows that as the taint changes to darker blotches in the frame the composition changes from Ni-rich species to a Titanium Rich species present in the alloy. This graph shows the presence of higher peaks for Titanium. The presence of oxygen can also be seen as an external agent which shows up due to sintering in atmospheric conditions and without vacuum.

ISSN No:-2456-2165

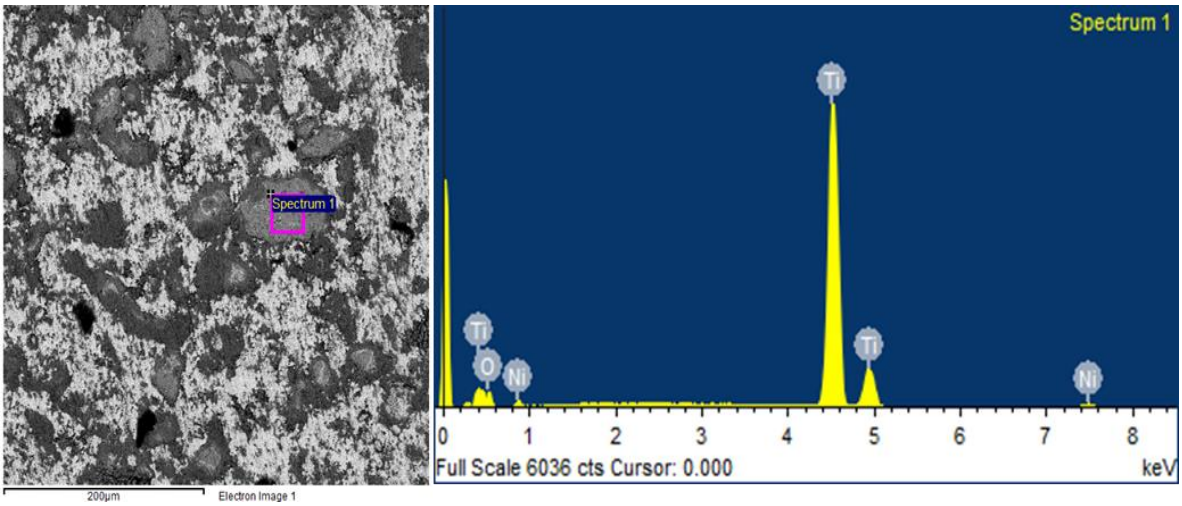

Fig. 16: SEM results of sample 1

This shows the presence of Ti as we focus over the spectrum to a less greyish taint which reflects the presence of different species present in the alloy and also maps with the historical context of judging the species using a color pattern from whitish to grey and then to black.

Batch A (Sample 2)

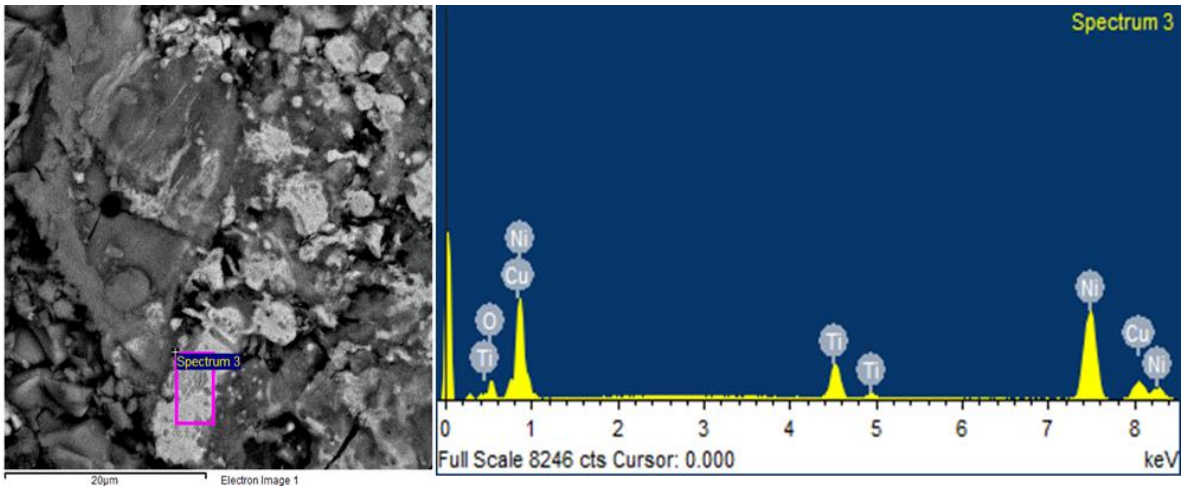

Fig. 17: SEM results of sample 2

This sample holds Cu alloy is the atomic percentage of 5 hence looking for the very images of it shows the presence of different species spread across the plane. When the focus was moved towards the whitish taint it reciprocates that the nature of species is Ni dominant also it does hold for Cu amount in it as well.

ISSN No:-2456-2165

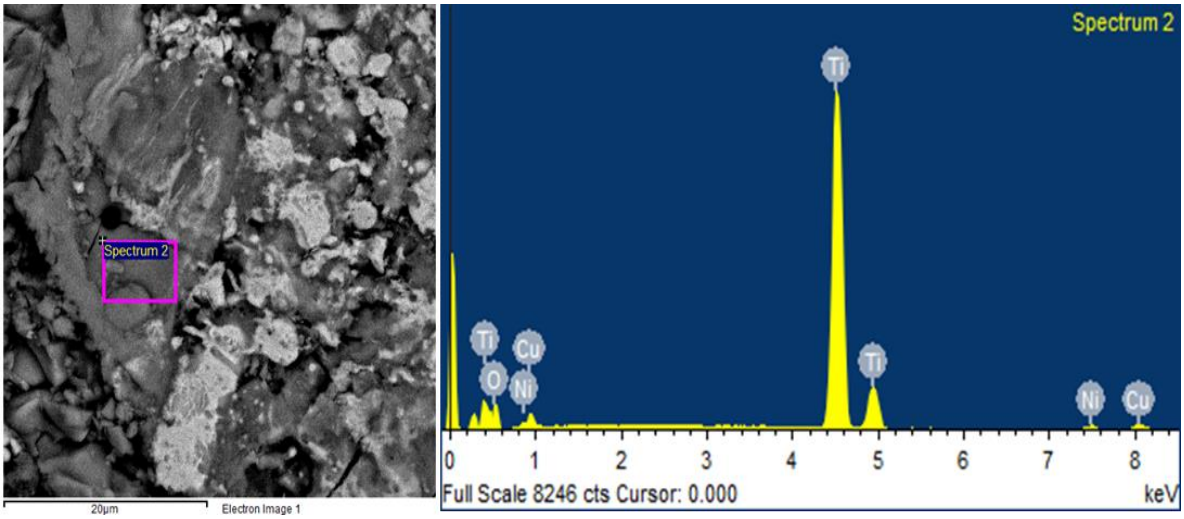

Fig. 18: SEM results of sample 2

For the greyish spectrum, the very nature of species is Ti-rich. The presence of H cannot be predicted using EDS but this element shows up in the XRD results. Also, a small amount of Cu and O can be seen in this focused spectrum of the image taken through FESEM TESCAN housed in the material department of IST, Islamabad.

D. DSC Results of Batch A Samples

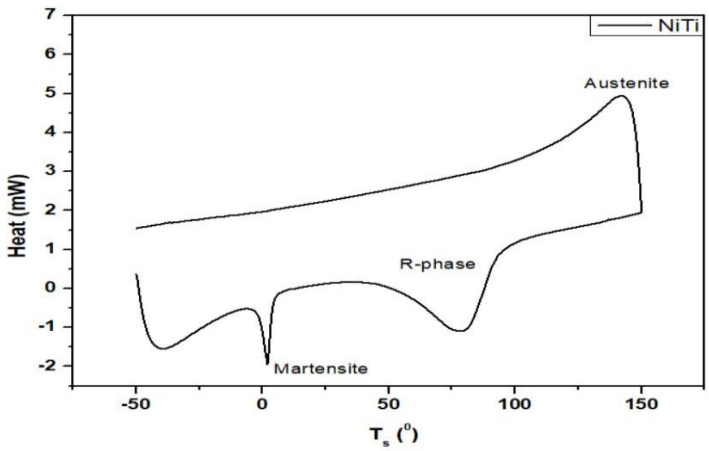

Fig. 19: DSC Results of Sample 1

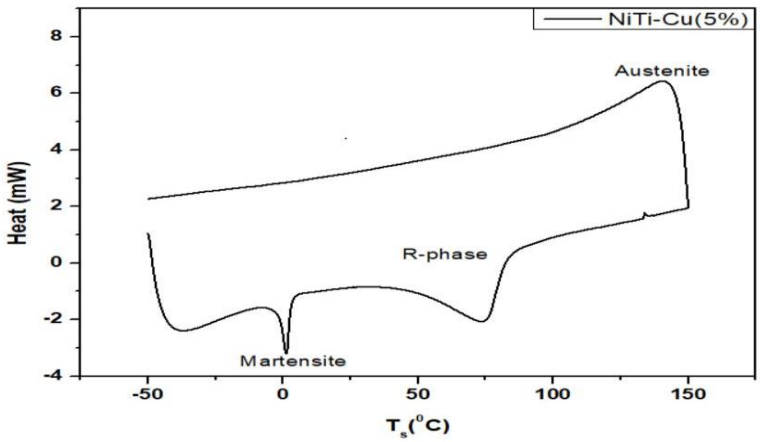

Fig. 20: DSC Results of Sample 2

ISSN No:-2456-2165

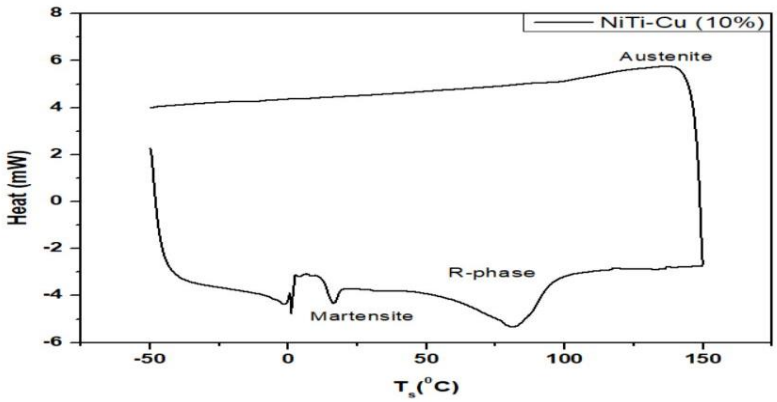

Fig. 21: DSC Results of Sample 3

DSC results show peaks in the endothermic process where the austenitic phase is achieved. Then this phase varies as the temperature rises above 120□ Celsius which is the austenite finish temperature. B2 cubic austenitic phase is achieved.

The addition of Cu in NiTi alloys causes the ternary alloys to exhibit thermal stability, lower sensitivity to stoichiometry. Hence, is implied in orthodontics. The addition of copper also defines the transition temperature which would ensure homogenous loading. Therefore, the stability of the dimensional properties is more consistent in the case of alloys with Cu as a ternary element.

E. Micro Hardness Test

Microhardness test has been performed on the first and second sample of batch A using ASTM E384-17 standard to measure the hardness and the results are as follows:

Table 6: Hardness value w.r.t Cu percentage

Cu %	Hardness Value
0	111
5	374

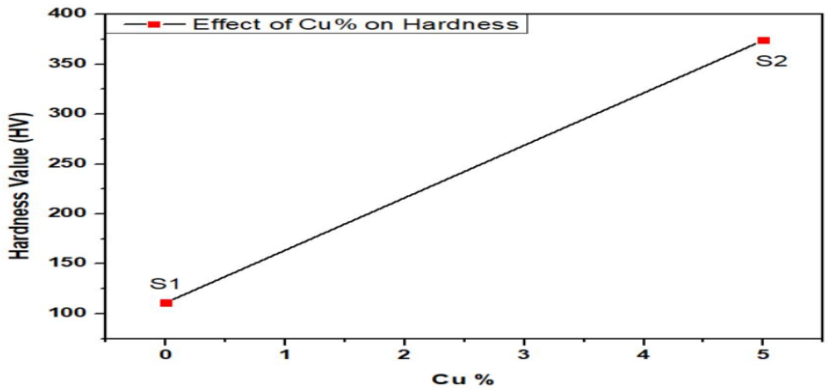

Fig. 22: Hardness value variation with Cu%

The addition of copper increases the hardness greatly from an average 100Hv to 400Hv for the comparison between samples 1 and 2 (Batch A).

IV. CONCLUSIONS

The powder metallurgy method produces more porous species as compared to SLM and DSLM. The variation in the porosity of alloys depends on the copper atomic percentage inside the species. The SMA effect is prominent in NiTi alloy and this effect starts to degrade with the inclusion of Cu in the alloy specimen. Sintering conditions play an important role in the species present in alloys. Alloys having NiTi phase also have other peaks hinting towards the presence of other species due to oxygen present in the sintering tube. The hardness of a shape memory alloy is also dependent on the copper addition inside the material. The trend shows an increase in hardness with the increase in the copper atomic percentage. EDS machining of the alloys presents that the machining is easier for Powder metal alloys, the right choice of pocket to hold the billets is necessary. Alloys can be made to shrink or expand in size in both the vertical and radial direction for the billets based on the variation in the sintering temperature and on the crucible used. Crucible used while sintering can induce certain lags in the dimensional accuracy of the specimen in case it starts to melt at higher temperatures.

REFERENCES

[1.] Adharapurapu, R. R., & Vecchio, K. S. (2007). Superelasticity in a new bioImplant material: Ni-rich 55NiTi alloy. Experimental Mechanics, 47(3), 365–371. https://doi.org/10.1007/s11340-006-9004-x

[2.] Alnomani, S. N., Zuheir Fadhel, E., & Mehatlaf, A. A. (2017). Prepare Nitinol Alloys and Improve their Hardness Using Copper as an Alloying Element. International Journal of Applied Engineering Research, 12(14), 4299–4308.

[3.] Arda, N. T., Hakan, G., & Bülent, B. (2018). Effect of Cu a ddition on m icrostructure and m echanical p roperties of NiTi b ased s hape m emory a lloy. 02(01), 20–26.

[4.] Ashrafi, M. J., Arghavani, J., Naghdabadi, R., & Auricchio, F. (2016). A three-dimensional phenomenological constitutive model for porous shape memory alloys including plasticity effects. Journal of Intelligent Material Systems and Structures, 27(5), 608–624. https://doi.org/10.1177/1045389X15575085

[5.] Atiyah, A. A., Ali, A. R. K. A., & Dawood, N. M. (2015). Characterization of NiTi and NiTiCu Porous Shape Memory Alloys Prepared by Powder Metallurgy (Part I). Arabian Journal for Science and Engineering, 40(3), 901–913. https://doi.org/10.1007/s13369-014-1538-0

[6.] Aydoğmus, T., & Bor, A. S. (2011). Production and characterization of porous TiNi shape memory alloys. Turkish Journal of Engineering and Environmental Sciences, 35(2), 69–82. https://doi.org/10.3906/muh-1007-127

[7.] Aydoğmuş, T., Bor, E. T., & Bor, Ş. (2011). Phase transformation behavior of porous TiNi alloys produced by powder metallurgy using magnesium as a space holder. Metallurgical and Materials Transactions A: Physical Metallurgy and Materials Science, 42(9), 2547–2555. https://doi.org/10.1007/s11661-011-0714-z

[8.] Bin Suleiman Ahmad, M. J., Bin Ahmad, M. A., Bin Ibrahim, R., Bin Mohamad, M., Abu Kasim, N. B., Bin Dato' Abdul Kadir, M. R., Bin Muhamad, S., Itoh, Y., Hanada, K., & Shimizu, T. (2013). Effect of sintering conditions on mechanical properties and microstructure of Titanium alloy produced by Metal Injection Moulding (MIM). Advanced Materials Research, 686, 164–169. https://doi.org/10.4028/www.scientific.net/AMR.686.164

[9.] Castillo, S. M., Muñoz, S., Trueba, P., Díaz, E., & Torres, Y. (2019). Influence of the compaction pressure and sintering temperature on the mechanical properties of porous titanium for biomedical applications. Metals, 9(12). https://doi.org/10.3390/met9121249

[10.] Fellah, M., Hezil, N., Touhami, M. Z., A. Hussien, M., Montagne, A., Mejias, A., Iost, A., Kossman, S., Chekalkin, T., Obrosov, A., & Weiss, S. (2020). Effect of Sintering Temperature on Mechanical and Tribological Behavior of Ti-Ni Alloy for Biomedical Applications. Minerals, Metals and Materials Series, February, 1701–1710. https://doi.org/10.1007/978-3-030-36296-6_157

[11.] Gil, F. J., Solano, E., Peña, J., Engel, E., Mendoza, A., & Planell, J. A. (2004). Microstructural, mechanical and cytotoxicity evaluation of different NiTi and NiTiCu shape memory alloys. Journal of Materials Science: Materials in Medicine, 15(11), 1181–1185. https://doi.org/10.1007/s10856-004-5953-8

[12.] Gupta, G. K., Patel, K. K., Purohit, R., & Bhagoria, P. (2017). Effect of Rolling on Ni-Ti-Fe Shape Memory Alloys Prepared Through Novel Powder Metallurgy Route. Materials Today: Proceedings, 4(4), 5385–5397. https://doi.org/10.1016/j.matpr.2017.05.050

[13.] Hori, K., Namazu, T., & Inoue, S. (2010). Effect of Cu content on the shape memory behavior of Ti-Ni-Cu alloy thin films prepared by triple-source dc magnetron sputtering. Thin Solid Films, 518(21 SUPPL.), S26–S28. https://doi.org/10.1016/j.tsf.2010.03.027

[14.] Imran Khan, M., Kim, H. Y., Nam, T. H., & Miyazaki, S. (2012). Formation of nanoscaled precipitates and their effects on the high-temperature shape-memory characteristics of a Ti 50Ni 15Pd 25Cu 10 alloy. Acta Materialia, 60(16), 5900–5913. https://doi.org/10.1016/j.actamat.2012.07.032

[15.] Jabur, A. S., Al-Haidary, J. T., & Al-Hasani, E. S. (2013). Characterization of Ni-Ti shape memory alloys prepared by powder metallurgy. Journal of Alloys and Compounds, 578, 136–142. https://doi.org/10.1016/j.jallcom.2013.05.029

[16.] Kahloul, L., Chadli, H., Beliardouh, N. E., & Bououdina, M. (2019). Cold pressing dependence on microstructure and electrochemical performance of porous TiNi alloy. Materials Research Express, 6(9). https://doi.org/10.1088/2053-1591/ab3023

[17.] Khalil-Allafi, J., & Amin-Ahmadi, B. (2009). The effect of chemical composition on enthalpy and entropy changes of martensitic transformations in binary NiTi shape memory alloys. Journal of Alloys and Compounds, 487(1–2), 363–366. https://doi.org/10.1016/j.jallcom.2009.07.135

[18.] Khan, M. I., Kim, H. Y., Namigata, Y., Nam, T. H., & Miyazaki, S. (2013). Combined effects of work hardening and precipitation strengthening on the cyclic stability of TiNiPdCu-based high-temperature shape memory alloys. Acta Materialia, 61(13), 4797–4810. https://doi.org/10.1016/j.actamat.2013.04.066

[19.] Khanlaria, K., Ramezani, M., Kelly, P., Cao, P., & Neitzert, T. (2018). Synthesis of As-sintered 60NiTi parts with a high open porosity level. Materials Research, 21(5), 1–12. https://doi.org/10.1590/1980-5373-MR-2018-0088

[20.] Kim, Y. W., & Jeon, K. S. (2010). Shape memory characteristics of powder metallurgy processed Ti 50Ni50 alloy. Physics Procedia, 10, 17–21. https://doi.org/10.1016/j.phpro.2010.11.068

[21.] Kocich, R., Szurman, I., & Kurs, M. (2013). The Methods of Preparation of Ti-Ni-X Alloys and Their Forming. Shape Memory Alloys - Processing, Characterization and Applications. https://doi.org/10.5772/50067
[22.] Liu, N., & Huang, W. M. (2006). DSC study on temperature memory effect of NiTi shape memory alloy. Transactions of Nonferrous Metals Society of China (English Edition), 16(SUPPL.). https://doi.org/10.1016/S1003-6326(06)60138-6
[23.] Losertová, M., Štencek, M., Matýsek, D., Štefek, O., & Drápala, J. (2017). Microstructure evolution of heat treated NiTi alloys. IOP Conference Series: Materials Science and Engineering, 266(1), 0–7. https://doi.org/10.1088/1757-899X/266/1/012008
[24.] Miyazaki, S. (2017). My Experience with Ti–Ni-Based and Ti-Based Shape Memory Alloys. Shape Memory and Superelasticity, 3(4), 279–314. https://doi.org/10.1007/s40830-017-0122-3
[25.] Nafari Q., M., & Abbasi, S. M. (2013). Influence of composition and thermomechanical training process on the transformation behavior and shape memory properties of NiTi based alloys. Transactions of the Indian Institute of Metals, 66(3), 239–245. https://doi.org/10.1007/s12666-013-0256-8
[26.] Phukaoluan, A., Dechkunakorn, S., Anuwongnukroh, N., Khantachawana, A., Kaewtathip, P., Kajornchaiyakul, J., & Wichai, W. (2017). Loading and unloading forces following addition of 5% Cu in nickel-titanium alloy used for orthodontics. Key Engineering Materials, 730 KEM, 161–166. https://doi.org/10.4028/www.scientific.net/KEM.730.161
[27.] Sadrnezhaad, S. K., Arami, H., Keivan, H., & Khalifezadeh, R. (2006). Powder metallurgical fabrication and characterization of nanostructured porous NiTi shape-memory alloy. Materials and Manufacturing Processes, 21(8), 727–735. https://doi.org/10.1080/10426910600727882
[28.] Sampath, V., Srinithi, R., Santosh, S., Sarangi, P. P., & Fathima, J. S. (2020). The Effect of Quenching Methods on Transformation Characteristics and Microstructure of an NiTiCu Shape Memory Alloy. Transactions of the Indian Institute of Metals, 73(6), 1481–1488. https://doi.org/10.1007/s12666-020-01909-9
[29.] Scalet, G., Conti, M., & Auricchio, F. (2017). Computational Analysis of Advanced Shape-Memory Alloy Devices Through a Robust Modeling Framework. Shape Memory and Superelasticity, 3(2), 109–123. https://doi.org/10.1007/s40830-017-0102-7
[30.] Sepe, V., Auricchio, F., Marfia, S., & Sacco, E. (2015). Micromechanical analysis of porous SMA. Smart Materials and Structures, 24(8). https://doi.org/10.1088/0964-1726/24/8/085035
[31.] Takemoto, Y., Shimizu, I., Sakakibara, A., Hida, M., & Mantani, Y. (2004). Tensile behavior and cold workability of Ti-Mo alloys. Materials Transactions, 45(5), 1571–1576. https://doi.org/10.2320/matertrans.45.1571
[32.] Wadood, A. (2016). Brief overview on nitinol as biomaterial. Advances in Materials Science and Engineering, 2016. https://doi.org/10.1155/2016/4173138
[33.] Wen, C., Yu, X., Zeng, W., Zhao, S., Wang, L., Wan, G., Huang, S., Grover, H., & Chen, Z. (2018). Mechanical behaviors and biomedical applications of shape memory materials: A review. In AIMS Materials Science (Vol. 5, Issue 4). https://doi.org/10.3934/matersci.2018.4.559
[34.] Wisutmethangoon, S., Denmud, N., Sikong, L., & Suttisripok, W. (2008). Influence of compaction pressure on the morphology and phase evolution of porous NiTi alloy prepared by SHS technique. Songklanakarin Journal of Science and Technology, 30(6), 761–765.
[35.] Yasenchuk, Y., Marchenko, E., Gunther, V., Radkevich, A., Kokorev, O., Gunther, S., Baigonakova, G., Hodorenko, V., Chekalkin, T., Kang, J. hoon, Weiss, S., & Obrosov, A. (2019). Biocompatibility and clinical application of porous tini alloys made by self-propagating high-temperature synthesis (SHS). Materials, 12(15). https://doi.org/10.3390/ma12152405
[36.] Yu, J. Y., & Li, Q. (2011). Study on effect of sintering temperature on microstructure and compressive property of porous NiTi alloys. Advanced Materials Research, 299–300, 480–483. https://doi.org/10.4028/www.scientific.net/AMR.299-300.480.